Force modelling of the crankshaft pin grinding process

A P Walsh[1]*, **B Baliga**[2] and **P D Hodgson**[1]
[1]Deakin University, Geelong, Victoria, Australia
[2]St Cloud State University, St Cloud, Minnesota, USA

Abstract: A force model was developed for crankshaft pin grinding to predict the forces generated during grinding. The force model developed builds on the authors' previously developed model, which predicted the out-of-roundness in crankshaft pin grinding. The model includes key grinding variables, such as the work removal parameter (WRP), system stiffness and Young's modulus to determine the end forces produced. The model also includes the important geometrical relationships that are unique to this type of grinding. The model was verified using an experiential set-up involving sophisticated strain gauge force measurements on a commercial Landis CP grinding machine, with close correlation between the results and the model.

Keywords: grinding, crankshaft, pin, force modelling

1 INTRODUCTION

It has been demonstrated in literature [**1**, **2**] that the forces generated in grinding contribute greatly to the finished product, which can affect the surface finish and part dimensions of the ground workpiece and lead to higher cycle times of the grinding operation. To overcome these problems an understanding of the grinding forces, and more importantly how to predict these forces, is required to optimize the process. A number of grinding force models have been developed in the past to predict the forces in grinding [**3**–**5**], such as the Peters chip model [**6**], which calculates the forces produced by the size of the theoretical grinding chip. The Malkin force model [**7**] uses empirical equations to predict the grinding forces by estimating the forces developed by each of the grits during cutting and then calculates the average force produced across the width of the grinding wheel.

Some drawbacks and limitations do exist with their implementation of these models, such as the tedious and time consuming task of counting the cutting grits on the grinding wheel, which is more suitable for laboratory studies than production environments. A vast majority of the force models developed are not very general and cannot handle the grinding of complex shapes and associated interactions that is required for crankshaft pin grinding. Thus the aim of the current work is to develop a force model appropriate for the geometric and process conditions in crankshaft pin grinding, which can easily be applied to production environments. The crankshaft pin grinding force models produced are verified experimentally.

The MS was received on 28 May 2003 and was accepted after revision for publication on 29 October 2003.
* *Corresponding author: Deakin University, Pigdons Road, Geelong, Victoria, Australia.*

2 CRANKSHAFT PIN FORCE GRIND MODELLING

The crankshaft pin force grinding model was developed into three parts and integrated for the final model. The first part determined the forces of the crankshaft pin generated by the straight face of the grinding wheel. The second part determined the forces developed by the corner radius of the grinding wheel and the third determined the forces arising from the residual elasticity of the grinding wheel travelling down the shoulder of the pin.

2.1 The grinding wheel face

2.1.1 Forces developed by the infeed stage

Cylindrical grinding consists of the given infeed of the grinding wheel feeding into the workpiece and the actual penetration infeed velocity or actual velocity being produced on the workpiece after allowing for deflections of the grinding system. This can be seen graphically in Fig. 1. The actual velocity at any point of time is given in the following equation, worked out previously by the

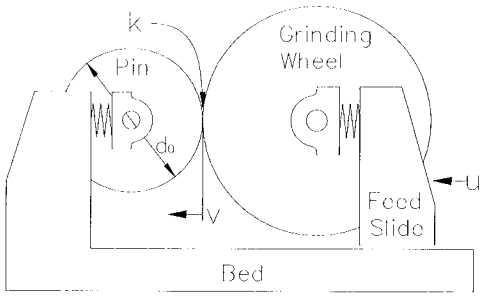

Fig. 1 A diagrammatic side on view representation of the crankshaft pin grinding process

author [**8**]:

$$v = \frac{\pi d_0 + tk\ \mathrm{WRP}' - \sqrt{\pi^2 d_0^2 + 2\pi d_0 tk\ \mathrm{WRP}' + t^2 k^2\ \mathrm{WRP}'^2 - 8\pi t^2 k\ \mathrm{WRP}' u}}{4\pi t} \tag{1}$$

where

v = actual velocity (mm/s)
WRP′ = work removal parameter per unit width (mm^3/s, N, mm)
k = system stiffness (N/mm)
d_0 = initial diameter (mm)
t = time during grinding wheel infeed (s)
u = given infeed velocity (mm/s)

The force produced at any point of time for cylindrical grinding is given by [**9**]

$$F = \frac{\pi d v b}{\mathrm{WRP}} \tag{2}$$

where

b = width of grinding wheel face (mm)
WRP = work removal parameter (mm^3/s, N)
$d = d_0 - 2R_{\mathrm{infeed}}$

R_{infeed} in equation (2) is the distance over time that the actual grinding velocity has travelled, which has been previously worked out by the author as [**8**]

$$\begin{aligned} R_{\mathrm{infeed}} = {} & \frac{1}{4} d_0 \ln(t) + \frac{tk\ \mathrm{WRP}' - A}{4\pi} - \frac{d_0 k\ \mathrm{WRP}' \ln[A(k\ \mathrm{WRP}' - 8\pi u) - \sqrt{B}(8t\pi u - tk\ \mathrm{WRP}' - \pi d_0)]}{4\sqrt{B}} \\ & + \frac{d_0 k\ \mathrm{WRP}'[2\ln(k\ \mathrm{WRP}' - 8\pi u) + 2\ln(\pi d_0 k\ \mathrm{WRP}' + \sqrt{\pi^2 d_0^2}\sqrt{B}) - \ln(B)]}{8\sqrt{B}} \\ & - \frac{d_0^2 \pi \left[-2 \arctan h\left(\frac{\sqrt{\pi^2 d_0^2} A}{\pi^2 d_0^2 + t\pi d_0 k\ \mathrm{WRP}'} \right) - 2 - \ln(2) + \ln(\pi) + 2\ln(d_0) - \ln(k) - \ln(\mathrm{WRP}') - \ln(u) \right]}{8\sqrt{\pi^2 d_0^2}} \end{aligned} \tag{3}$$

where

$$A = \sqrt{\pi^2 d_0^2 + 2t\pi d_0 k\ \mathrm{WRP}' - 8t^2 \pi k\ \mathrm{WRP}' u + t^2 k^2\ \mathrm{WRP}'^2}$$

$$B = k^2\ \mathrm{WRP}'^2 - 8\pi k\ \mathrm{WRP}' u$$

The width of the grinding wheel face is given by

$$b = w - 2(R_1 + s) \tag{4}$$

where

w = width of the grinding wheel (mm)
R_1 = corner radius of the crankshaft pin (mm)
s = shoulder width of material to be removed from one side of the crankshaft pin (mm)

Combining equations (1), (2) and (4) gives the normal force at any point of time during the infeed:

$$F = \frac{(d_0 - 2R_{\text{infeed}})(\pi d_0 + tk\ \text{WRP}' - \sqrt{\pi^2 d_0^2 + 2\pi d_0 tk\ \text{WRP}' + t^2k^2\ \text{WRP}'^2 - 8\pi t^2 k\ \text{WRP}'u})[w - 2(R_1 + s)]}{4t\ \text{WRP}} \quad (5)$$

2.1.2 *Forces developed by the sparkout stage*

Sparkout velocity occurs when the given infeed of the grinding wheel has stopped and the actual infeed velocity keeps going due to deflection in the grinding system. This has also been worked out previously by the author [**8**] and is shown as

$$v_s = \frac{v\pi d_s}{\pi d_s + tk\ \text{WRP}'} \quad (6)$$

where

v_s = sparkout velocity (mm/s)
d_s = diameter of the crankshaft pin at the start of the sparkout (mm)
t_s = amount of sparkout time (s)

Combining equations (2) and (6) gives the normal force at any point of time during the sparkout:

$$F = \frac{\pi^2 v d_s b(d_s - 2R_{\text{sparkout}})}{(\pi d_s + tk\ \text{WRP}')\ \text{WRP}} \quad (7)$$

where $b = w - \varepsilon_1$ (mm); ε_1 is determined in equation (41). R_{sparkout} in equation (7) is the distance over time that the actual sparkout velocity has travelled, which has been previously worked out by the author [**8**] as

$$R_{\text{sparkout}} = \frac{\ln(\pi d_s + tk\ \text{WRP}')v\pi d_s}{k\ \text{WRP}'} - \frac{v\pi d_s[\ln(\pi) + \ln(d_s)]}{k\ \text{WRP}'} \quad (8)$$

2.2 The corner radius of the grinding wheel

From the author's work [**8**] there are two corner geometrical models that can be represented for crankshaft pin grinding. The first geometric model is where the corner radius of the crankshaft pin is greater or equal to the corner radius of the grinding wheel minus the shoulder width:

Crankshaft pin corner geometrical model one:

$$R_1 \geqslant R_2 - s \quad (9)$$

The second geometric model is where the corner radius of the crankshaft pin is less than the corner radius of the grinding wheel minus the shoulder width:

Crankshaft pin corner geometrical model two:

$$R_1 < R_2 - s \quad (10)$$

where

R_2 = corner radius of the grinding wheel

For the purpose of this paper the first model will be used where the radius of the grinding wheel is greater or equal to the radius of the crankshaft pin minus the shoulder width, which is most commonly used in industry. Figure 2 shows the geometrical model of the grinding wheel radius grinding down the side of the crankshaft pin, which is based on this case. The crankshaft pin radius model is broken into various subsections, as shown in the following equations. Figure 2 demonstrates a step-by-step procedure that is needed for this particular model; close examination of the diagram shows that the model is broken down into segments as parts 1, 2 and 3. The steps required for each segment are shown as descending alphabetical letters. Because each segment and step is different they all need to be looked at individually in order to study the forces being produced during grinding, and are later combined to obtain the total force. Also note that actual force grinding times start at 1B and not 1A, as this is the point where contact is made between the grinding wheel and the crankshaft pin. The force equations for each of the steps are summarized as follows:

Step 1A

The forces produced at this stage are 0.

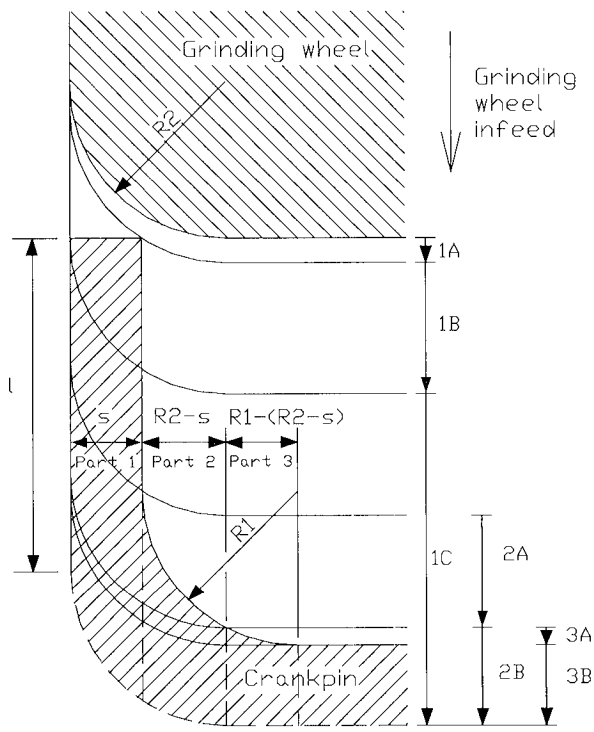

Fig. 2 Top view of the geometrical relationships for the radius grind model

Step 1B

$$F = \frac{2\pi(d_0 - 2R_{\text{infeed}})(\pi d_0 + tk\ \text{WRP}' - \sqrt{\pi^2 d_0^2 + 2\pi d_0 tk\ \text{WRP}' + t^2k^2\ \text{WRP}'^2 - 8\pi t^2 k\ \text{WRP}'u}) \times [\sqrt{R_2^2 - (\sqrt{2R_2 s - s^2} - R_{\text{infeed}})^2} - (R_2 - s)]}{4\pi t\ \text{WRP}}$$

Step 1C

$$F = \frac{2\pi(d_0 - 2R_{\text{infeed}})(\pi d_0 + tk\ \text{WRP}' - \sqrt{\pi^2 d_0^2 + 2\pi d_0 tk\ \text{WRP}' + t^2k^2\ \text{WRP}'^2 - 8\pi t^2 k\ \text{WRP}'u})(s - \varepsilon_1)}{4\pi t\ \text{WRP}}$$

Step 2A

$$F = \frac{2\pi(d_0 - 2R_{\text{infeed}})(\pi d_0 + tk\ \text{WRP}' - \sqrt{\pi^2 d_0^2 + 2\pi d_0 tk\ \text{WRP}' + t^2k^2\ \text{WRP}'^2 - 8\pi t^2 k\ \text{WRP}'u})b}{4\pi t\ \text{WRP}}$$

where

$$b = (2AR_2^2 + 2s(3R_2R_1s - s^2R_1 - 2R_2^2R_1 + sA - sR_1^2 + R_2R_{\text{infeed}}^2 - 2R_{\text{infeed}} + 2R_2R_1^2) + R_{\text{infeed}}^2(R_1^2 - R_2^2 - s^2) - 2AR_1^2 - (\sqrt{2R_2s - s^2} - R_{\text{infeed}})\sqrt{-1 \times (R_1 - R_2 + s)^2[4R_1s(-2R_2R_1 + R_1s - 2A) + R_{\text{infeed}}^2(4R_1s - 4R_2R_1 + R_{\text{infeed}}^2 + 8R_2s - 4A - 4s^2) + 8R_1R_2A]}$$
$$(2R_1^2 + 2R_{\text{infeed}}^2 + 2R_2^2 - 4R_2R_1 - 4A + 4R_1s)(R_1 - R_2 + s)$$

where

$$A = \sqrt{2R_2s - s^2}R_{\text{infeed}}$$

Step 2B

$$F = \frac{2\pi(d_0 - 2R_{\text{infeed}})(\pi d_0 + tk\ \text{WRP}' - \sqrt{\pi^2 d_0^2 + 2\pi d_0 tk\ \text{WRP}' + t^2k^2\ \text{WRP}'^2 - 8\pi t^2 k\ \text{WRP}'u})(R_2 - s)}{4\pi t\ \text{WRP}}$$

Step 3A

$$F = \frac{2\pi[(d_0 - 2R_{\text{infeed}} - 2(R_2 - \sqrt{2R_2s - s^2})] \times (\pi d_0 + tk\ \text{WRP}' - \sqrt{\pi^2 d_0^2 + 2\pi d_0 tk\ \text{WRP}' + t^2k^2\ \text{WRP}'^2 - 8\pi t^2 k\ \text{WRP}'u})b}{4\pi t\ \text{WRP}}$$

where

$$b = [R_1 - (R_2 - s)] - \sqrt{R_1^2 - (\sqrt{2R_1R_2 - 2R_1s - R_2^2 + 2R_2s - s^2} + R_{\text{infeed}})^2}$$

Step 3B

$$F = \frac{2\pi[d_0 - 2R_{\text{infeed}} - 2(R_2 - \sqrt{2R_2s - s^2})] \times (\pi d_0 + tk\ \text{WRP}' - \sqrt{\pi^2 d_0^2 + 2\pi d_0 tk\ \text{WRP}' + t^2k^2\ \text{WRP}'^2 - 8\pi t^2 k\ \text{WRP}'u})[R_1 - (R_2 - s)]}{4\pi t\ \text{WRP}}$$

The total force contributed by the corner infeed of the grinding wheel is

$$F = \text{steps 1A and 3B summed together (during their engaged period)} \tag{11}$$

2.3 Residual elasticity on the shoulder

Because a grinding wheel contains some degree of elasticity, the residual elasticity also needs to be determined after the infeed stage of the grinding wheel on the side of the crankshaft pin, much like the sparkout stage needs to be determined by the face of the grinding wheel.

A diagram to represent the residual elasticity of the side of the grinding wheel is shown in Fig. 3. It has been shown that Young's modulus can be used to determine the deflection of the grinding wheel when grinding [**10**, **11**]. The deflection in the grinding wheel is caused

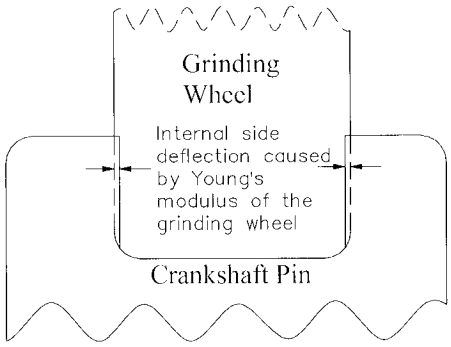

Fig. 3 Elasticity of the grinding wheel on the side of the crankshaft pin

by the elasticity of the wheel, illustrated in Fig. 3. To determine the forces produced, the relationship between Young's modulus is first identified:

$$E = \frac{\sigma}{\varepsilon} \tag{12}$$

where

E = Young's modulus (N/mm^2)
σ = stress (N/mm^2) = force/area
ε = strain ($\Delta L/L$)
L = half the grinding wheel width (mm)
ΔL = amount of deflection (mm)

The force can be represented by the relationship between system stiffness and deflection as

$$F = \varepsilon_1 K \tag{13}$$

where

F = force (N)
ε_1 = deflection (mm)
K = system stiffness constant (N/mm)

As $\varepsilon_1 = \Delta L = \varepsilon L$, equation (13) can be rewritten as

$$K = \frac{F}{\varepsilon L} \tag{14}$$

Combining equations (12) and (14) leads to

$$K = \frac{EF}{\sigma L} \tag{15}$$

Equation (15) can also be rewritten as

$$K = \frac{E \times \text{area}}{L} \tag{16}$$

Substituting equation (16) into (13) leads to

$$F = \frac{\varepsilon_1 E \times \text{area}}{L} \tag{17}$$

Rearranging equation (17) in terms of deflection yields

$$\varepsilon_1 = \frac{FL}{E \times \text{area}} \tag{18}$$

The next step requires obtaining the sparkout velocity contributed by Young's modulus of the grinding wheel on the side of the shoulder of the crankshaft pin. From the author's previous work [**8**] the correlation between the sparkout velocity and initial deflection is as follows:

$$\varepsilon_s = -v_{ss} t + c \tag{19}$$

where

ε_s = deflection during the sparkout stage (mm)
v_{ss} = sparkout velocity for the shoulder
c = initial deflection

The force in grinding has the following relationship developed by Hahn and Richard [**9**]:

$$F = \frac{Q}{\text{WRP}} \tag{20}$$

where

Q = material removal rate (mm^3/s) = area $\times$ v
WRP = work removal parameter

Combining equations (18), (19) and (20) and simplifying gives the following:

$$\frac{v_{ss} L}{\text{WRP}} = -v_{ss} t + \varepsilon_1 \tag{21}$$

Rearranging equation (21) to obtain the sparkout velocity gives

$$v_{ss} = \frac{\varepsilon_1 \text{WRP}}{L + t\,\text{WRP}} \tag{22}$$

Equation (20) is combined with equation (22) and simplified to determine the forces produced on the shoulder of the crankshaft pin at any one point of time:

$$F = \frac{\text{area} \times \varepsilon_1}{L + t\,\text{WRP}} \tag{23}$$

Since the force acts in the perpendicular direction to the normal force the normal and tangential forces must be found. The force correlation is as follows:

$$F_n = \frac{F_t}{\lambda} \tag{24}$$

where

λ = friction constant between the contact of the grinding wheel and the crankshaft pin

To find the total normal force in the direction of the grinding wheel contributed by the elasticity of the wheel, equation (23) is combined with equation (24) and multiplied by 2 (two shoulders), leading to

$$F = \frac{2 \times \text{area} \times \varepsilon_1 \lambda}{L + t\,\text{WRP}} \tag{25}$$

The area in equation (25) is worked out using the following steps. To find the grinding area of the side of

the shoulder at any one point of time Fig. 4 will be used to determine the geometric relationships. For the crankshaft pin shoulder,

$$C^2 = b^2 + h_1^2 \tag{26}$$

where

C = radius of the crankshaft pin shoulder (mm)
b = half the bisecting intersection width (mm)
h_1 = distance from the bisecting intersection to the centre of the crankshaft pin radius (mm)

For the grinding wheel,

$$G^2 = b^2 + h_2^2 \tag{27}$$

where

G = radius of the grinding wheel (mm)
b = half the bisecting intersection width (mm)
h_2 = distance from the bisecting intersection to the centre of the grinding wheel radius (mm)

Combining equations (26) and (27) leads to

$$C^2 - h_1^2 = G^2 - h_2^2 \tag{28}$$

From Fig. 4, the following geometric relationship is established:

$$h_1 + h_2 = C + G - R_{\text{infeed}} \tag{29}$$

Combining equations (28) and (29) and solving leads to

$$h_1 = \frac{2C^2 + 2CG - 2CR_{\text{infeed}} - 2GR_{\text{infeed}} + R_{\text{infeed}}^2}{2(C + G - R_{\text{infeed}})} \tag{30}$$

Combining equations (28) and (29) and solving leads to

$$h_2 = \frac{2G^2 + 2CG - 2CR_{\text{infeed}} - 2GR_{\text{infeed}} + R_{\text{infeed}}^2}{2(C + G - R_{\text{infeed}})} \tag{31}$$

The area created by the crankshaft pin shoulder is

$$A_1 = \frac{\arccos(h_1/C)}{180}\pi C^2 - \sqrt{C^2 - h_1^2}h_1 \tag{32}$$

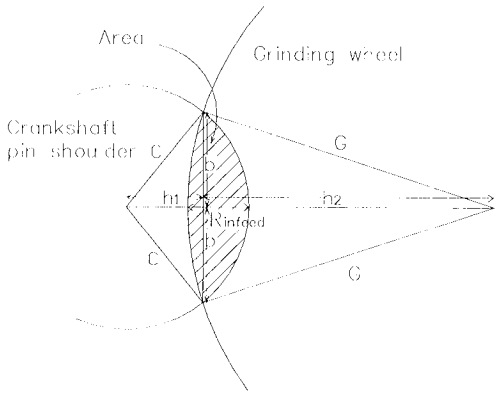

Fig. 4 The area of shoulder being ground

The area created by the grinding wheel is

$$A_2 = \frac{\arccos(h_2/G)}{180}\pi G^2 - \sqrt{G^2 - h_2^2}h_2 \tag{33}$$

The total area grinded on the shoulder at any point of time by the infeed is

$$\text{Area} = (A_1 + A_2) \tag{34}$$

It should also be noted that when grinding has reached the sparkout out stage, the infeed actual velocity in equation (34) will be converted to the sparkout velocity from equation (6).

The ε_1 in equation (25) is worked out using the following steps. First the perpendicular distance produced to the shoulder from the corner radius of the grinding wheel going into the crankshaft pin is found, using the parallel given infeed over a function of time. From Fig. 2, the following geometric relationship can be made:

$$p = \sqrt{R_2^2 - (\sqrt{2R_2s - s^2} - ut)^2} - R_2 + s \tag{35}$$

where

p = perpendicular distance travelled (mm)

The next step is to find the given velocity that is perpendicular to the shoulder produced from the corner radius of the grinding wheel going into the crankshaft pin. This is done by differentiating equation (35) with respect to time and is shown by

$$p_u = \frac{(\sqrt{2R_2s - s^2} - ut)u}{\sqrt{R^2 - (\sqrt{2R_2s - s^2} - ut)^2}} \tag{36}$$

where

p_u = perpendicular given velocity

From the author's previous work [8] a correlation exists between the given velocity, actual velocity and deflection. This is shown as

$$\varepsilon_1 = (p_u - v_p)t + C \tag{37}$$

where

v_p = actual perpendicular velocity
$C = 0$, as there is no initial deflection

Combining equations (17), (20), (36) and (37) and solving for v leads to

$$v_p = \frac{(\sqrt{2R_2s - s^2} - ut)utE\,\text{WRP}}{\sqrt{R_2^2 - (\sqrt{2R_2s - s^2} - ut)^2}(L + tE\,\text{WRP})} \tag{38}$$

The time needed for the given velocity to reach the end of the corner radius of the grinding wheel on to the side of the crankshaft pin is given by

$$t = \frac{\sqrt{2R_2s - s^2}}{u} \tag{39}$$

Equation (38) is integrated with respect to time, from $t = 0$ to $t =$ equation (39), to determine the actual perpendicular distance travelled over the set time period:

$$R_{\text{perpendicular}} = -[-u^3E^3\,\text{WRP}^3R_2\sqrt{A} - u^2E\,\text{WRP} - L\ln(B)u^4E^2\,\text{WRP}^2\sqrt{2R_2s - s^2} - L^2\ln(B)u^5E\,\text{WRP} + u^3E^3\,\text{WRP}^3\sqrt{r^2 - 2R_2s + s^2}\sqrt{A} - Lu^4E^2\,\text{WRP}^2\arctan \times \left(\frac{\sqrt{2R_2s - s^2}}{\sqrt{R_2^2 - 2R_2s + s^2}}\right)\sqrt{A} + Lu^4E^2\,\text{WRP}^2\sqrt{2R_2s - s^2}\ln(2) + Lu^4E^2\,\text{WRP}^2\frac{\sqrt{2R_2s - s^2}\ln(D) + L^2u^5E\,\text{WRP}\ln(2) + L^2u^5E\,\text{WRP}\ln(D)]}{E^3\,\text{WRP}^3u^3\sqrt{A}} \quad (40)$$

where

$$A = -\frac{u^2L^2 + 2\sqrt{2R_2s - s^2}uLE\,\text{WRP} - R_2^2E^2\,\text{WRP}^2 + (2R_2s - s^2)E^2\text{WRP}^2}{E^2\,\text{WRP}^2}$$

$$B = -2\frac{-R_2^2E\,\text{WRP} - \sqrt{A}R_2E\,\text{WRP}}{\sqrt{2R_2s - s^2}E\,\text{WRP}/u + L}$$

$$D = \frac{-\sqrt{2R_2s - s^2}uL + R_2^2E\,\text{WRP} - (2R_2s - s^2)E\,\text{WRP} + \sqrt{A}\sqrt{R_2^2 - 2R_2s + s^2}E\,\text{WRP}}{L}$$

The elastic deflection of the grinding wheel is the shoulder width minus $R_{\text{perpendicular}}$:

$$\varepsilon_1 = s - R_{\text{perpendicular}} \quad (41)$$

2.4 Total forces contributed by the grinding wheel

The total forces contributed by the grinding wheel are equations (5), (7), (11) and (25) combined together.

3 EXPERIMENTAL

The required data to validate the force crankshaft pin grinding models experimentally were obtained on a Landis 6 pin cylindrical crankshaft pin grinder using a Norton 53A54LVS specified grinding wheel. Placement of strain gauges on the tail stock, head stock and work support allowed the forces to be measured during grinding. The analogue signals from the strain gauges were converted to digital signals and then converted to computer format by a data-logging card. The data were later processed to a force reading. The experimental validation and force simulation used the variables shown in Table 1. The test used a single plunge grinding cycle with one infeed and a 10 s sparkout.

4 RESULTS AND DISCUSSION

Results of the forces measured during the grinding cycle of the crankshaft pin are shown in Fig. 5, with the predicted grinding forces from the grinding model. From Fig. 5, the model results show close agreement with the measured forces during crankshaft pin grinding. In the initial stage there are no forces produced until the leading radial edge of the grinding wheel corner touches the shoulder of the pin. Once the wheel starts grinding the shoulder, both results are in agreement with each other. Halfway down the shoulder the measured forces tend to be marginally higher than the calculated results. Both the calculated force and measured force show approximately the same position and force slope generated when the corner radius and face of the grinding wheel starts grinding the stock of the crankshaft pin. Both results are indicated above 400 N during face grinding of the crankshaft pin, which then drops off when the wheel feed stops and sparkout begins. The model was also verified by the use of two other specifications of grinding wheels, one a harder grade wheel (M) with a determined WRP value of 0.82 $\text{mm}^3/\text{s, N}$ and one a softer grade grinding wheel (K) with a determined WRP value of 0.64 $\text{mm}^3/\text{s, N}$. The results of the theoretical and measured forces are shown in Fig. 6. The other important variable in the grinding model is also the system stiffness value, again verification of the grinding model was completed by using three different system stiffness values represented by a high stiffness value of pin 1 (4136 N/mm) near the headstock and then along the crankshaft to pin 2 (3082 N/mm) and then pin 3 (1975 N/mm), which is near the centre of the crankshaft. The results of the theoretical and measured forces from the different system stiffness values are shown in Fig. 7. From Fig. 6, there is quite a significant difference in the force generated on the crankshaft pin for the different WRP values. A high WRP value or easy cutting wheel generates low forces compared to a lower WRP value or a harder wheel. From Fig. 6, the theoretical and measured forces do show similar results, with the measured force dropping off slightly more from a higher WRP value. From Fig. 7, there appears only to be a slight drop in forces between the high system stiffness value and the low system stiffness value. It should also be noted that a reduction in system

Table 1 Values of the variables used during the grinding force measurements

Description	Symbol	Value	Unit
Corner radius of the crankshaft pin	R_1	2.5	mm
Corner radius of the grinding wheel	R_2	2.5	mm
Shoulder to be ground	s	0.23	mm
Initial diameter including the shoulder	d_0	64.8132	mm
Rough stock on the crankshaft pin face		0.7	mm
Finish diameter on the crankshaft pin face		53.944	mm
Work removal parameter	WRP	0.69	mm^3/s, N
Work removal parameter per unit width	WRP′	0.0272	mm^3/s, N, mm
System stiffness	k	4136	N/mm
Given infeed velocity	u	0.067	mm/s
Young's modulus	E	18 000	N/mm^2
Half width of the grinding wheel	L	12.7	mm
Width of the grinding wheel	w	25.4	mm
Width of the crankshaft pin face		24.97	mm
Radius of the crankshaft pin	C	32.4066	mm
Radius of the grinding wheel	G	500	mm
Friction constant	λ	0.35	

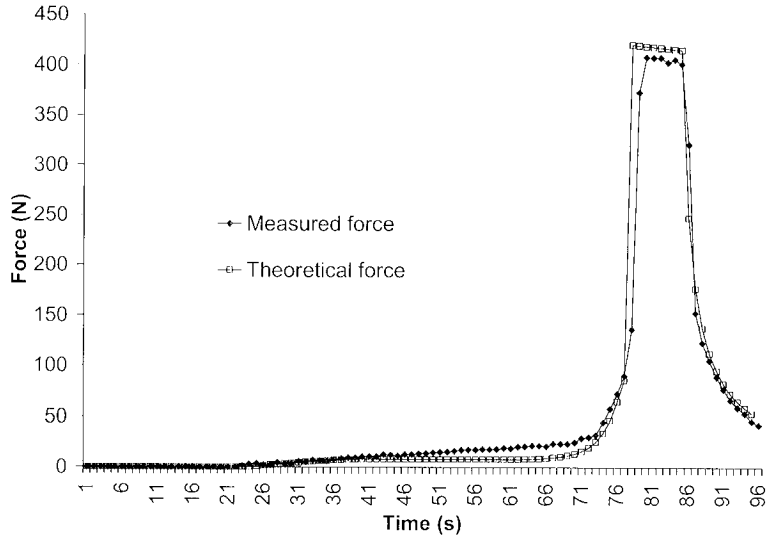

Fig. 5 The experimental and predicted grinding force results

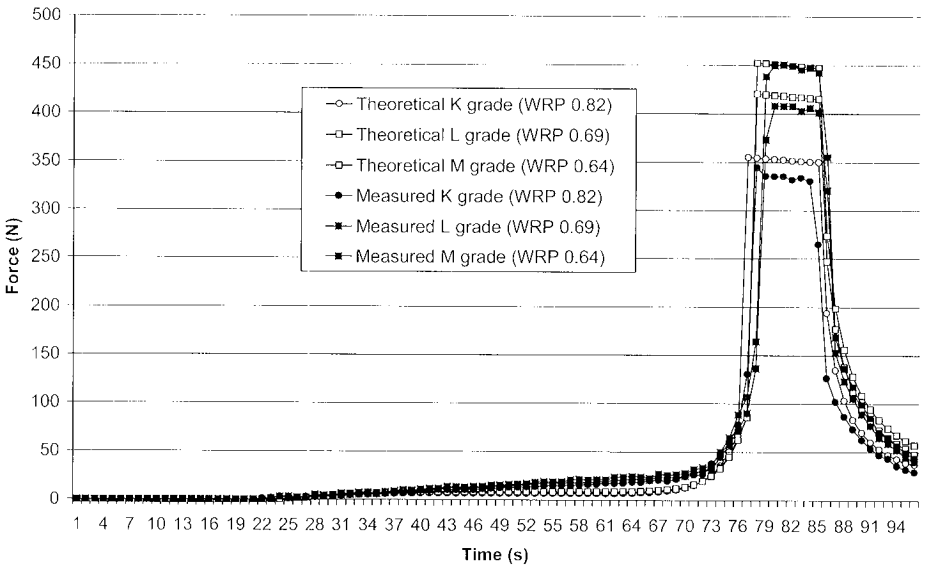

Fig. 6 Theoretical and measured forces from different wheel grades (WRP values)

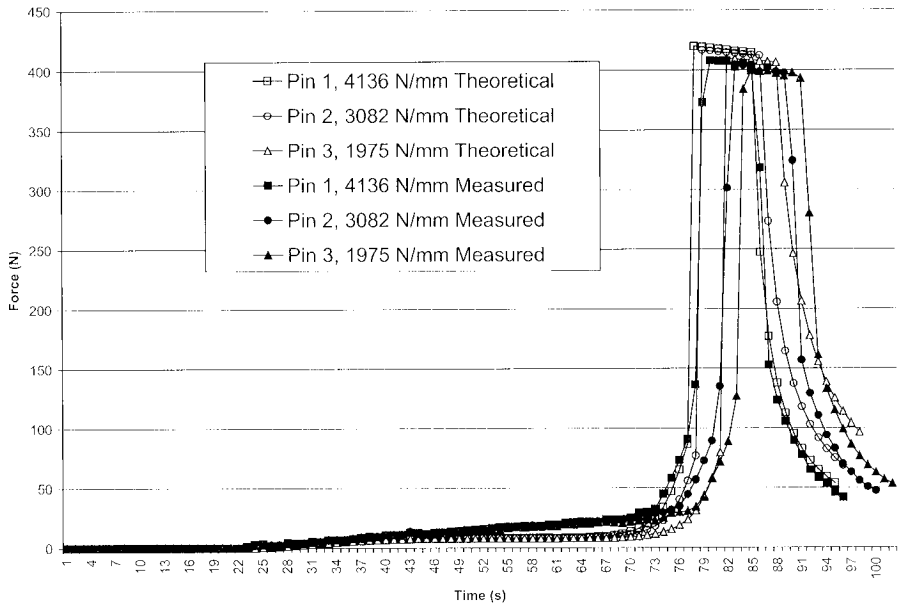

Fig. 7 Theoretical and measured forces from different pins along the crankshaft (system stiffness values)

stiffness also decreases the actual grinding velocity produced and hence the actual distance being ground, which explains why the lower system stiffness values in Fig. 7 take longer to grind the crankshaft pin than the higher values. Again from Fig. 7, the measured forces show a similar pattern to those of the theoretical forces, with the exception of the measured forces having lower values during the sparkout stage, especially with the lower system stiffness value of pin 3. This might indicate instability in the model if values are too low.

5 CONCLUSION

Force modelling of the crankshaft pin grinding process requires an understanding of the complex geometrical relationships and key grinding variables that underpin the operation. It was shown that the crankshaft pin model predicted results were in agreement with the experimentally observed results. The force grinding model produced is very suitable for production applications in crankshaft pin grinding, giving the grinding engineer confidence that the grinding force model developed will greatly assist in optimizing their grinding operation.

ACKNOWLEDGEMENTS

The authors wish to thank the Ford Motor Company of Australia for their ongoing support and providing access to production machinery and test equipment. One of the authors (Aaron Walsh) acknowledges the scholarship support from the Australian Research Council and Ford Motor Company of Australia.

REFERENCES

1 **Brach, K. P. D. M., Ratterman, E.** and **Shaw, M. C.** Grinding forces and energy. *Trans. ASME, J. Engng for Industry*, 1988, **110**(February), 25–31.

2 **Ono, K.** Analysis on the grinding force. *Bull. JSGE*, 1961, **1**, 19–22.

3 **Von Salje, E. I.** Grundlagen des Schleifvorganges. *Werkstatt und Betr.*, 1953, **86**(4), 177–182.

4 **Werner, G.** Influence of work material on grinding forces. In *Grinding: Theory, Techniques and Troubleshooting* (Ed. R. C. L. Bhateja), 1978, pp. 89–94 (Society of Manufacturing Engineers, Dearborn, Michigan).

5 **Tonshoff, H. K. P. J., Inasaki, I.** and **Paul, T.** Modelling and simulation of grinding processes. *Ann. CIRP*, 1992, **41**(2), 677–688.

6 **Peters, J. S. R.** and **Decneut, A.** The proper selection of grinding conditions in cylindrical plunge grinding. In *Grinding: Theory, Techniques and Troubleshooting* (Ed. R. C. L. Bhateja), 1978, pp. 107–114 (Society of Manufacturing Engineers, Dearborn, Michigan).

7 **Malkin, S.** *Grinding Technology Theory and Applications of Machining with Abrasives*, 1989, p. 275 (Society of Manufacturing Engineers, Dearborn, Michigan).

8 **Walsh, A. P.** Mathematical modeling of the crankshaft pin grinding process. Preprint PhD thesis, Deakin University, 2003.

9 **Hahn, R. S. L.** and **Richard. P.** Principles of grinding. In *Grinding: Theory, Techniques and Troubleshooting* (Ed. R. C. L. Bhateja), 1971, pp. 3–41 (Society of Manufacturing Engineers, Dearborn, Michigan).

10 **Kumar, K. V. S. M. C.** The role of wheel work deflection in grinding operations. *Trans. ASME, J. Engng for Industry*, 1981, **103**(February), 73.

11 **Sauer, J. W. S.** and **Milton, C.** The role of elastic deflections of the wheel work interface in surface grinding. Proceedings of the International Conference of Production Engineers, 1974.